JOURNAL OF PROPULSION AND POWER
Vol. 11, No. 3, May–June 1995

Computation of Turbulent Reacting Flow in a Solid-Propellant Ducted Rocket

Yei-Chin Chao,* Wen-Fuh Chou,† and Sheng-Shyang Liu‡
National Cheng Kung University, Tainan, Taiwan 701, Republic of China

A mathematical model for computation of turbulent reacting flows is developed under general curvilinear coordinate systems. An adaptive, streamline grid system is generated to deal with the complex flow structures in a multiple-inlet solid-propellant ducted rocket (SDR) combustor. General tensor representations of the k-ε and algebraic stress (ASM) turbulence models are derived in terms of contravariant velocity components, and modification caused by the effects of compressible turbulence is also included in the modeling. The clipped Gaussian probability density function is incorporated in the combustion model to account for fluctuations of properties. Validation of the above modeling is first examined by studying mixing and reacting characteristics in a confined coaxial-jet problem. This is followed by study of nonreacting and reacting SDR combustor flows. The results show that Gibson and Launder's ASM incorporated with Sarkar's modification for compressible turbulence effects based on the general curvilinear coordinate systems yields the most satisfactory prediction for this complicated SDR flowfield.

Nomenclature

C_{g1}, C_{g2} = constants in Eq. (11)
C_{pi} = isobaric specific heat
C_{r1}, C_{r2} = constants in ASM
C_1, C_2, C_D, C_μ = constants in the k-ε model
$\hat{e}^i$ = contravariant base vector with unit length
f = mixture fraction
G_g = production term in Eq. (11)
G_k = production rate of turbulent kinetic energy defined in Eqs. (5) and (8)
g = variance of mixture fraction
g^{ij} = metric tensor
J = Jacobian
k = turbulent kinetic energy
P = mean pressure
P_k = production rate of turbulent kinetic energy for unit mass
r = stoichiometric air-fuel mass ratio
S_ϕ = source term in Eq. (13)
T = temperature
U, V = mean Cartesian velocity components
U^i = mean contravariant velocity components
$U(i)$ = mean physical contravariant velocity components
$\boldsymbol{U}$ = mean velocity vector
u^i = fluctuation of mean contravariant velocities
v^i = fluctuation of mean Cartesian velocities
X, Y = Cartesian coordinate
x^k = general curvilinear coordinate
Y_i = mass fraction of species i
Γ^i_{jk} = Christoffel symbol of second kind
Γ_ϕ = effective exchange coefficient in Eq. (13)
ε = turbulence energy dissipation rate
μ = viscosity
ρ = density
τ = stress tensor excluding pressure term
ϕ = flow variable in Eq. (13)

Subscripts
A = properties of air feed
eff = sum of laminar and turbulent parts
F = properties of fuel feed
f = properties of fuel
in = properties of inert species
st = stoichiometric values
t = turbulent part
0 = properties of oxidant

Superscript
$\bar{}$ = time-mean quantities

Received Dec. 9, 1993; revision received Aug. 25, 1994; accepted for publication Sept. 1, 1994.

*Professor, Institute of Aeronautics and Astronautics. Member AIAA.
†Research Assistant, Institute of Aeronautics and Astronautics.
‡Research Assistant, Institute of Aeronautics and Astronautics. Member AIAA.

Introduction

RESEARCH of solid-propellant ducted rockets (SDR) has received a great deal of attention in the modern development of propulsion systems. In comparison with solid-fuel ramjets and liquid-fuel ramjets, SDR has several advantages, such as simplicity in fuel management, throttle ability of fuel flow rates, minimum problems in terms of flammability, etc. In a typical SDR combustor module, airstreams enter the combustor chamber through multiple side inlets, and the fuel-gas streams are injected from the head-end dome plate. The complicated turbulent flow in the SDR combustor can be regarded as a combination of a number of flow characteristics, including free jets, jet-to-jet impingement, reattachments, recirculations, and boundary-layer flows. The interaction of these flow characteristics contributes to the turbulent mixing and the reacting processes in the SDR combustor. It is important to conduct basic research on these complicated interaction phenomena in order to better utilize and design SDR systems.

In experimental investigations, Schadow[1,2] studied the ignition problem of various fuels used in the SDR, including nonmetalized and boron particle-laden propellants. Schadow concluded that high efficiency could be obtained if the gas-phase combustion can be initiated near the fuel injection nozzle. Zetterström et al.[3,4] conducted combustion tests with both propane fuel and a solid propellant, and found that the combustion behavior associated with these two fuels is quite sim-

ilar. Flow visualizations were conducted by Stull et al.[5] and Nosseir and Behar.[6] Liou and Wu[7] applied the LDV system to measure mean velocities and turbulence quantities in an isothermal dual-inlet, side-dump combustor. To further study the flow patterns in SDR, Chuang[8] applied both LDV measurements and schlieren flow visualizations to observe the isothermal and reacting SDR flowfields.

In contrast to experimental investigations, analytical tools now available for design optimization and performance prediction of SDR are still far from satisfactory. Direct numerical simulation with three-dimensional time-dependent partial differential equations is time consuming, and perhaps one might say, formidable. Current models applied to computations of SDR flows are restricted to Cartesian or cylindrical coordinates.[9-11] The adequacy of grid arrangement and the induced numerical diffusion error in this complicated flowfield require further evaluation. Body-fitted coordinate systems have been widely used for predicting flows with complex geometries. However, for flow characteristics induced mainly by the interaction of flows themselves rather than by complex boundary geometries, the body-fitted coordinate system may produce grid lines that are skewed with respect to flow directions. As for turbulence modeling, most researchers[9,10] apply the k-ε model to evaluate turbulent stresses. Liou and Hwang[11] noticed anisotropic turbulence characteristics in the actual SDR flows and adopted an algebraic stress model for flowfield prediction. For the SDR operation, the additional effects of compressible turbulence (which may result from high-speed flow interaction due to sonic fuel gas injection and side inlets or chemical reactions), have not been included in SDR flow computations. The suitability of the incompressible version of turbulence models for SDR flow computations is open to question.

Combustion modeling poses another difficulty. Because complete chemical kinetics are very complicated for many practical fuels, researchers often simplify the chemical reaction steps. Some investigations[12,13] indicated that the mixing controlled assumption is satisfactory for engineering purposes. In the case of high Reynolds number flows, the presence of turbulence helps to enhance the mixing of fuels with the oxidizer, thus promoting combustion efficiency. The heat release during the combustion process in turn changes the density and turbulent structure of the flowfield. Chen and Tao[9] adopted a simplified scheme that assumes an infinitely fast one-step global reaction. Cherng et al.[10] further investigated the combustion process by assuming two-step, chemical kinetics with a modified eddy break-up model in both two- and three-dimensional SDR model combustors. Since the actual turbulence-chemistry interaction is still not well understood, the fluctuations of properties are generally solved by assuming the shape of the probability density function (PDF). Spalding's[14] choice of a periodic form of PDF for the fluctuations of mixture fraction makes it possible to calculate mean values of species concentration, temperature, density, and other fluid properties. In general, results obtained in the prediction of concentration fields were good even though unrealistic peaks were observed in the temperature profiles. For more realistic fluctuation modes, a triangular waveform and a beta function distribution were proposed by Naguib[15] and Richardson et al.,[16] respectively. It was found that the unrealistic temperature peaks no longer exist with these PDF shapes. Since much experimental evidence[17,18] suggests that the turbulence fluctuations of properties are essentially random in character, Naguib[15] assumed the PDF to be a clipped Gaussian distribution bounded by two delta functions. This model, used by Elghobashi[19] and Khalil,[20] obtained better results.

In view of the deficiencies in previous research in the simulation of the complicated SDR flow, further investigation of the anisotropic turbulence model based on a streamline adaptive grid system is performed in this work. To better predict the turbulent reacting SDR flowfield, modification due to the effects of compressible turbulence and incorporation of clipped Gaussian PDF accounting for property fluctuations are included in this prediction.

Theoretical Formulation

In order to facilitate the mathematical analysis of the complicated turbulent reacting SDR flow, several assumptions are made. The flow is assumed to be steady, with negligible body force and radiative heat transfer. The combustion is assumed to be infinitely fast and to have a global one-step with a unity Lewis number. Adiabatic solid wall boundaries are also assumed.

Based on the general curvilinear coordinates, mean flow properties are governed by the Navier-Stokes equation with Reynolds-averaging. To close the momentum equations, the Reynolds stress is formulated through turbulence modeling. Both the k-ε and algebraic stress models are adopted in this work.

k-ε Model

In the k-ε two-equation model, the Reynolds stress is linked to the strain rate of the mean flowfield through Boussinesq's eddy viscosity concept. The expression of Reynolds stress in terms of contravariant velocity components is

$$\tau^{ij}_{t,k-\varepsilon} = \mu_t \left(g^{jk} \frac{\partial U^i}{\partial x^k} + g^{ik} \frac{\partial U^j}{\partial x^k} - U^k \frac{\partial g^{ij}}{\partial x^k} \right) - \frac{2}{3} g^{ij} \left[\frac{\mu_t}{J} \frac{\partial}{\partial x^k} (JU^k) + \rho k \right] \tag{1}$$

where

$$\mu_t = C_\mu \rho k^2/\varepsilon \tag{2}$$

And the transport of k and ε are governed by the following two equations, respectively:

$$\nabla\cdot(\rho \boldsymbol{U} k) - \nabla\cdot(\Gamma_k \nabla k) = G_k - \rho\varepsilon \tag{3}$$

$$\nabla\cdot(\rho \boldsymbol{U} \varepsilon) - \nabla\cdot(\Gamma_\varepsilon \nabla \varepsilon) = (C_1 G_k - C_2 \rho\varepsilon)(\varepsilon/k) \tag{4}$$

The term G_k in Eqs. (3) and (4) denotes the production rate of turbulent kinetic energy resulting from interaction of the Reynolds stress and the gradient of the mean flowfield, i.e.,

$$G_k = \bar{\bar{\tau}}_{t,k-\varepsilon} : \nabla \boldsymbol{U} \tag{5}$$

Algebraic Stress Model (ASM)

In contrast to the isotropic turbulence character in the k-ε modeling, the Reynolds stress is solved directly in the algebraic stress modeling. Rodi's approximation[21] is used here; i.e., the local value of $\overline{u^i u^j}/k$ is assumed to be spatially invariant, or its gradient is assumed to be very small. Under this approximation, the transport of Reynolds stress is proportional to that of turbulent kinetic energy. Thus, the Reynolds stress transport equation can be reduced to an algebraic form. In the general curvilinear coordinate system, Reynolds stress is expressed as

$$\tau^{ij}_{t,\mathrm{ASM}} = -\rho\overline{u^i u^j} \tag{6}$$

where

$$\frac{\overline{u^i u^j}}{k} = -\left(\overline{u^i u^k} \frac{\partial U^j}{\partial x^k} + \overline{u^j u^k} \frac{\partial U^i}{\partial x^k} \right) \frac{1 - C_{r2}}{P_k + C_{r1}\varepsilon - \varepsilon} + \frac{2}{3} \frac{C_{r2} P_k + C_{r1}\varepsilon - \varepsilon}{P_k + C_{r1}\varepsilon - \varepsilon} g^{ij} - (\overline{u^i u^k} U^m \Gamma^j_{mk} + \overline{u^j u^k} U^m \Gamma^i_{mk}) \frac{1 - C_{r2}}{P_k + C_{r1}\varepsilon - \varepsilon}$$

P_k indicates the production rate of turbulent kinetic energy per unit mass, i.e.,

$$P_k = G_k/\rho \tag{7}$$

G_k is the source term of the k-equation, and can be calculated by

$$G_k = \bar{\bar{\tau}}_{t,\mathrm{ASM}} : \nabla \boldsymbol{U} \tag{8}$$

Since the expression of Reynolds stress in the ASM is essentially a point function, not directly related to the surrounding nodes, the numerical calculation may suffer from instability problems. It is helpful to maintain the convective-diffusive nature of momentum equations as is done in formulation by the k-ε modeling. An artificial diffusion term $\nabla\cdot(\bar{\bar{\tau}}_{\mathrm{eff},k-\varepsilon})$ is introduced into the momentum equations as

$$\nabla\cdot(\rho\boldsymbol{UU}) = -\nabla P + \nabla\cdot(\bar{\bar{\tau}}_{\mathrm{eff},k-\varepsilon}) + \nabla\cdot(\bar{\bar{\tau}}_{\mathrm{eff,ASM}} - \bar{\bar{\tau}}_{\mathrm{eff},k-\varepsilon}) \tag{9}$$

In the calculation, $\nabla\cdot(\bar{\bar{\tau}}_{\mathrm{eff},k-\varepsilon})$ is treated as a diffusion term and $\nabla\cdot(\bar{\bar{\tau}}_{\mathrm{eff,ASM}} - \bar{\bar{\tau}}_{\mathrm{eff},k-\varepsilon})$ is treated as a source term. Note that the expression of the momentum equations reduces to the form in the k-ε modeling if the source term diminishes. This treatment of momentum equations with the inclusion of the terms of the k-ε model lessens the instability in the calculation with the ASM significantly.

Turbulent Combustion Modeling

In a two-feed system, with the assumption of equal transport coefficients for reactants and products, the instantaneous species mass fraction can be expressed in terms of explicit functions of the mixture fraction. The mixture fraction f is defined by

$$\frac{(Y_f - Y_0/r) - (Y_f - Y_0/r)_A}{(Y_f - Y_0/r)_F - (Y_f - Y_0/r)_A} \tag{10}$$

where $(Y_f - Y_0/r)$ is the selected Shvab-Zeldovich coupling function.

For turbulent flows with mixing processes, the existence of turbulence results in significant fluctuations of properties, and special closure methods are needed. The conservation form of the mean mixture-fraction transport equation can be obtained with Reynolds averaging, and the transport equation of the variance of mixture fraction g is expressed as

$$\nabla\cdot(\rho\boldsymbol{U}g) - \nabla\cdot(\Gamma_g\nabla g) = C_{g1}G_g - C_{g2}\rho g(\varepsilon/k) \tag{11}$$

where the production term G_g is modeled with the eddy-viscosity concept as

$$G_g = \mu_t\nabla\bar{f}\cdot\nabla\bar{f} \tag{12}$$

For an adiabatic system with unity Lewis number, the equation and the boundary conditions of the total enthalpy are identical to those of the mixture fraction. Therefore, it is necessary only to solve the mixture fraction. Instantaneous temperature can be expressed as an implicit function of the mixture fraction through the specific heat relation $Cp_i(T)$. Instantaneous density of mixture gas can be calculated from the instantaneous form of the perfect gas law in terms of the mixture fraction for a given pressure. Mean values of these passive scalars are calculated through a presumed shape of the probability density function of the mixture fraction.

Two kinds of PDF are tested in this work. One is the double-Delta function PDF[14] which assumes rectangular-wave variations, and the other is the clipped Gaussian distribution PDF,[15] which assumes basically random fluctuations. The parameters in these presumed forms of PDF are determined by the mean and variance of the mixture fraction. Correspondence tables are constructed in advance to facilitate the searching algorithm during actual flow computations for calculation of the two parameters of clipped Gaussian PDF, the most probable value, and the standard deviation.

Representation of Transport Equations in General Tensor Form

As is the case with the above turbulence and combustion models, the transport equations of flow properties can be represented by a common form:

$$\frac{\partial}{\partial x^k}(J\rho U^k\phi) - \frac{\partial}{\partial x^k}\left(J\Gamma_\phi g^{jk}\frac{\partial\phi}{\partial x^j}\right) = JS_\phi \tag{13}$$

The dependent variables ϕ and the corresponding source terms S_ϕ for k-ε modeling are given in Table 1, and for ASM in Table 2. It is noted that all the velocity components formulated in the source terms are contravariant components U^i. The physical contravariant velocities $U(i)$ in the momentum equations defined below are chosen as dependent variables for ease of understanding their physical meaning:

$$U(i) \equiv \hat{\boldsymbol{e}}^i\cdot\boldsymbol{U} = U^i/\sqrt{g^{ii}} \tag{14}$$

The advantage in the present formulas of considering physical contravariant velocities as dependent variables (along with the consistency of all the velocity-related terms, including the convection and the source terms) eliminates the need for additional computation. Likewise, the expression of wall function derived by Chao and Liu[22] in terms of contravariant velocity components is adopted for calculation of the near-wall region. Application of contravariant velocity components in the nonuniform streamline grid system has been shown to be satisfactory by Chao and Liu[22] for cases of laminar and turbulent backward-step flows and turbulent jet in-cross flow.

Boundary Conditions

Properties of the near-wall regions are resolved by the law-of-the wall.[22,23] Zero-gradient condition is used at the symmetry axis for all dependent variables except the turbulent shear stress, which is designated as zero. The outlet position of the computational domain is set far enough to achieve a fully developed flow characteristic, and the zero-gradient con-

Table 1 Source terms of governing equations for k-ε model

ϕ	Γ_ϕ	$\sqrt{g^{ii}}S_\phi$
1	0	0
$U(i)$	μ_{eff}	$-\rho U^jU^k\Gamma^i_{jk} - g^{ij}\dfrac{\partial P}{\partial x^j} + \tau^{jk}_{\mathrm{eff}}\Gamma^i_{jk}$
		$+\dfrac{1}{J}\dfrac{\partial}{\partial x^k}\left[J\mu_{\mathrm{eff}}\left(g^{ij}\dfrac{\partial U^k}{\partial x^j} - U^j\dfrac{\partial g^{ik}}{\partial x^j}\right)\right]$
		$-\dfrac{1}{J}\dfrac{\partial}{\partial x^k}\left\{\dfrac{2}{3}Jg^{ik}\left[\dfrac{\mu_{\mathrm{eff}}}{J}\dfrac{\partial}{\partial x^j}(\rho U^j) + \rho k\right]\right\}$
		$-\rho U^kU^i\dfrac{\partial g^{ii}}{\partial x^k}\Big/2g^{ii}$
		$+\dfrac{1}{J}\dfrac{\partial}{\partial x^k}\left(J\mu_{\mathrm{eff}}g^{jk}U^i\dfrac{\partial g^{ii}}{\partial x^j}\Big/2g^{ii}\right)$
		$+g^{jk}\mu_{\mathrm{eff}}\dfrac{\partial U(i)}{\partial x^j}\dfrac{\partial\sqrt{g^{ii}}}{\partial x^k}$
k	$\mu_{\mathrm{eff}}/\sigma_k$	$\sqrt{g^{ii}}(G_k - C_D\rho\varepsilon)$
ε	$\mu_{\mathrm{eff}}/\sigma_\varepsilon$	$\sqrt{g^{ii}}(C_1G_k - C_2\rho\varepsilon)(\varepsilon/k)$
$\bar{f}$	$\mu_{\mathrm{eff}}/\sigma_f$	0
g	$\mu_{\mathrm{eff}}/\sigma_g$	$\sqrt{g^{ii}}[C_{g1}G_g - C_{g2}\rho g(\varepsilon/k)]$

Note: dependent variables for momentum equations are physical contravariant velocities.

Table 2 Source terms of governing equations for ASM

ϕ	Γ_ϕ	$\sqrt{g^{ii}}S_\phi$
1	0	0
$U(i)$	μ_{eff}	$-\rho U^j U^k \Gamma^i_{jk} - g^{ij}\frac{\partial P}{\partial x^j} + \tau^{jk}_{\text{eff}}\Gamma^i_{jk}$
		$+\frac{1}{J}\frac{\partial}{\partial x^k}\left[J\mu_{\text{eff}}\left(g^{ij}\frac{\partial U^k}{\partial x^j} - U^j\frac{\partial g^{ik}}{\partial x^j}\right)\right]$
		$-\frac{1}{J}\frac{\partial}{\partial x^k}\left\{\frac{2}{3}Jg^{ik}\left[\frac{\mu_{\text{eff}}}{J}\frac{\partial}{\partial x^j}(\rho U^j) + \rho k\right]\right\}$
		$-\rho U^k U^i \frac{\partial g^{ii}}{\partial x^k}\Big/ 2g^{ii}$
		$+\frac{1}{J}\frac{\partial}{\partial x^k}\left(J\mu_{\text{eff}}g^{ik}U^i\frac{\partial g^{ii}}{\partial x^j}\Big/ 2g^{ii}\right)$
		$+g^{jk}\mu_{\text{eff}}\frac{\partial U(i)}{\partial x^j}\frac{\partial\sqrt{g^{ii}}}{\partial x^k}$
		$+\frac{1}{J}\frac{\partial}{\partial x^k}[J(\tau^{ki}_{\text{eff,ASM}} - \tau^{ki}_{\text{eff},k-\varepsilon})]$
		$+\Gamma^i_{jk}[\tau^{jk}_{\text{eff,ASM}} - \tau^{jk}_{\text{eff},k-\varepsilon}]$
k	$\mu_{\text{eff}}/\sigma_k$	$\sqrt{g^{ii}}(G_k - C_D\rho\varepsilon)$
ε	$\mu_{\text{eff}}/\sigma_\varepsilon$	$\sqrt{g^{ii}}(C_1G_k - C_2\rho\varepsilon)(\varepsilon/k)$
$\tilde{f}$	$\mu_{\text{eff}}/\sigma_f$	0
g	$\mu_{\text{eff}}/\sigma_g$	$\sqrt{g^{ii}}[C_{g1}G_g - C_{g2}\rho g(\varepsilon/k)]$

Note: dependent variables for momentum equations are physical contravariant velocities.

dition is used for all dependent variables. In addition, a compensation strategy is applied to the axial velocity component to ensure mass conservation. Boundary conditions for inlets are prescribed according to experimental data.

Numerical Techniques

Transport equations in the form of Eq. (13) are discretized on the computational domain by the finite-volume method. A staggered grid system is employed. Although it is considered straightforward to use high-order difference schemes to reduce the truncation error, Shyy et al.[24] suggested that the effect of high-order schemes should be re-examined in the context of general coordinates. Calculations by Shyy et al.[24] with the hybrid, QUICK, and the second-order upwind difference schemes in a body-fitted coordinate system showed that the hybrid scheme yields the smallest mass residual of the three. Shyy et al.[24] also concluded that the choice of schemes is less important than the choice of the grid distribution. Therefore, the hybrid difference scheme is used in this work because of its superior stability in the curvilinear coordinates. To decouple the pressure-velocity relation in the momentum equations, the SIMPLEC algorithm[25] is adopted, with some modification for application in curvilinear coordinates. The coefficient matrix of the discretized system in the original pressure correction equation, which has a nine-point relationship when the Cartesian or the contravariant velocity components are chosen as the dependent variables,[24,26] becomes nondiagonally dominant and unstable. The stability problem can be removed by dropping the terms of cross-derivatives for pressure correction[24,26] in the velocity correction formulation. This approximation results in a five-point relationship for pressure correction that allows use of the iterative procedure. The SIMPLEC algorithm was also applied in a previous paper by Chao and Liu[22] in the curvilinear coordinates in terms of contravariant velocities for similar flow characteristics of turbulent back-step and jet in-cross flows. The convergence criterion is defined such that the maximum total normalized residual among all the discretized equations is less than 10^{-3} for the nonreacting flow case and 10^{-4} for the reacting flow case.

As discussed previously, one of the reasons for involving the curvilinear coordinate system as the basis of the present theoretical model is to reduce numerical errors caused by misalignment of the grid line with respect to flow streamline. The streamline adaptive grid method proposed by Chao and Liu[22] is adopted in this work.

To apply the streamline adaptive grid generation, a flow pattern predicted by a Cartesian grid system should be obtained in advance in order for generation of the stream function field to be performed. In the flowfield, the cross section with the most violent variation of flow properties is selected for grid generation, using the equidistribution scheme.[27] The degree of grid clustering is determined according to the variation of chosen flow properties with respect to a prescribed weighting function. The stream-function data is stored after grid generation for the corresponding new grids, and the new grids that correspond to the stored stream-function data at each axial grid line are found by interpolation. The new grids, each of which corresponds to stream-function data, form a streamline grid distribution. However, if there is a recirculation zone in the flowfield, there will be problems due to the closed-streamline pattern. The problems can be overcome by choosing two "dividing" streamlines to enclose the recirculation region and by assigning each grid a "pseudo" stream function via an equipartition process inside these two streamlines.

Results and Discussion

Computation of turbulent combustion in a cylindrical furnace is performed first to assess the theoretical analysis and numerical methods addressed previously. Following that, the turbulent nonreacting and reacting flowfields in an SDR combustor are studied.

Turbulent Combustion in a Cylindrical Furnace

Confined coaxial jets in a cylindrical furnace are studied here to evaluate the above theoretical formula. The cylindrical furnace used by Lockwood et al.,[28] which consists of coaxial jets and a sudden wall expansion, is adopted in the present study. Mixture fraction data were measured[28] at a number of axial locations for flow conditions at the Reynolds number of 1.603×10^4 and the fuel-air ratio of 0.0635. Computations for this test case are made using a 40×30 Cartesian grid system that clusters grids near walls and in regions inside the flame. Inlet boundary conditions are set to be uniform. Calculations with both the k-ε model and ASM are implemented. Model constants used in the ε equation are $C_1 = 1.45$, $C_2 = 2$ proposed by Hanjalic and Launder,[29] and the model constants used in the ASM, $C_{r1} = 1.5$, $C_{r2} = 0.6$, proposed by Launder et al.[30]

Results of calculations with the k-ε model are addressed first. Measurements of mixture fraction[28] and calculations without PDF and with the double-Delta function PDF are shown in Figs. 1a, 1b, and 1c, respectively. Results from predictions using the clipped Gaussian PDF are not presented because there are no significant differences between them and the double-Delta function PDF. In this figure, the location of the contour $\tilde{f} = 0.087$ corresponds to the stoichiometric flame sheet location. The measured flame length is about 700 mm, and the predictions with and without PDF are 600 and 1000 mm, respectively. Simulation with PDF in the calculation leads to a faster decay of turbulent flame length. Figure 2 shows the predicted temperature distributions along the centerline. An unrealistic peak is observed in the result of the double-Delta function PDF prediction. This phenomenon is believed to come from oversimplification of the property fluctuation in the double-Delta PDF. The unrealistic temperature peak can be removed by using the clipped Gaussian PDF. These results indicate that prediction of the mixture fraction

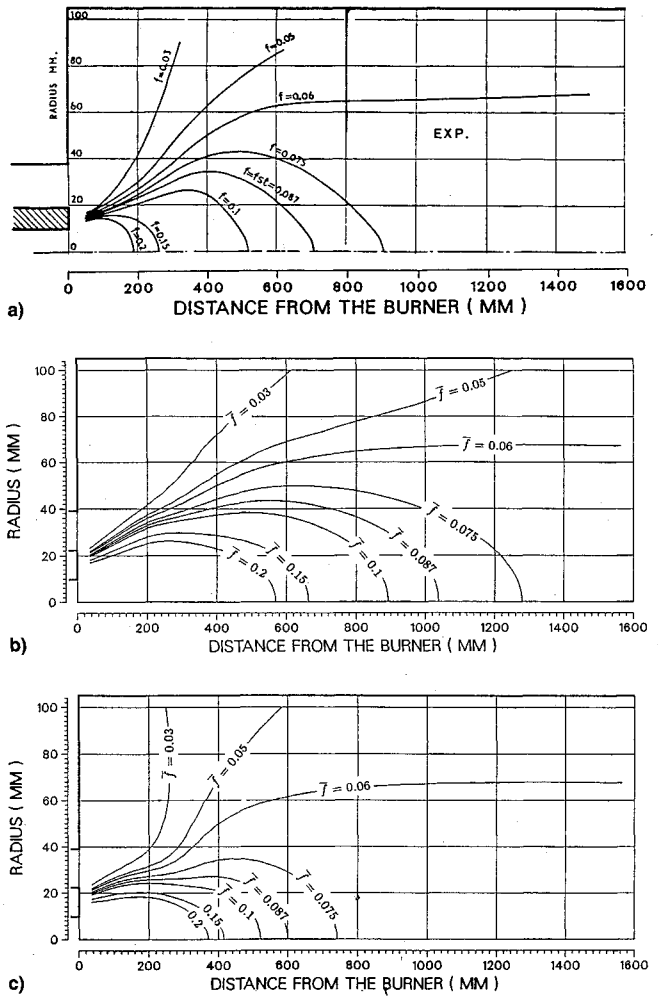

Fig. 1 Distributions of the mixture fraction in a cylindrical furnace: a) measurements[27]; b) prediction, not involving PDF; and c) prediction, involving PDF.

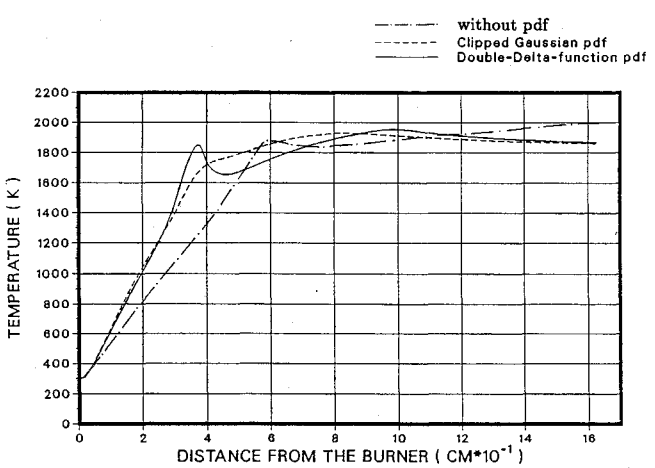

Fig. 2 Comparison of predicted temperature distributions, without PDF and with different types of PDF along the centerline of the furnace.

is not significantly influenced by the presumed shape of PDFs, but the temperature is.

To account for the anisotropic turbulence feature, calculations are performed using the algebraic stress model. Comparison of the predictions of mixture fraction by the ASM and the k-ε model is shown in Figs. 3a and 3b. Both models have been combined with the clipped Gaussian PDF to include the effects of property fluctuations in the predictions. The

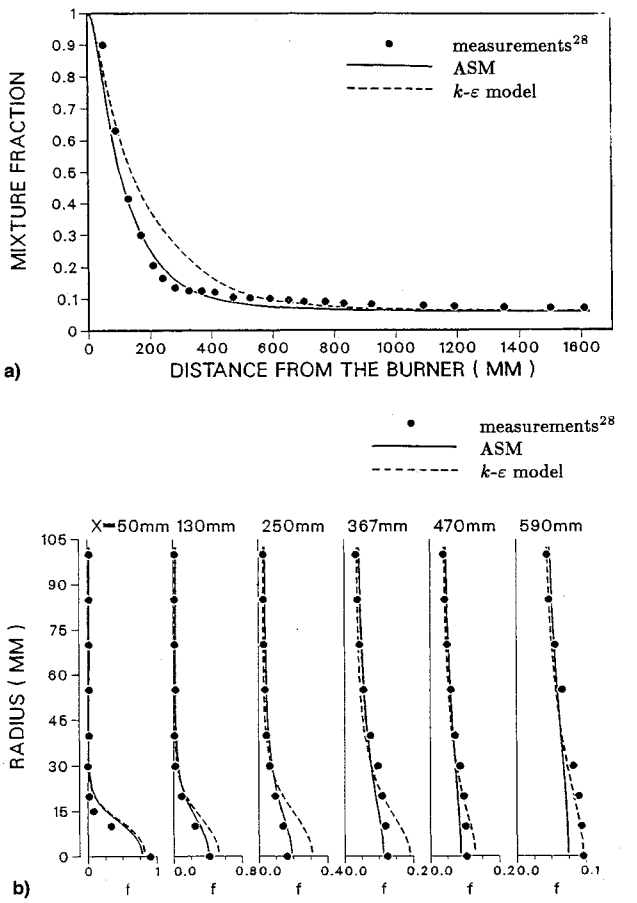

Fig. 3 Comparisons between predicted mixture fraction by different turbulence models and measured data[27]: a) distribution along centerline of furnace and b) radial distribution at different cross sections.

predictions of mixture fraction by the ASM match experiments much more closely than do those with the k-ε model along both axial and radial directions. This appears to be the result of a more accurate representation of the anisotropic turbulence in turbulent reacting flows.

In general, the present calculations of turbulent reacting flow in a cylindrical furnace are satisfactory with respect to actual experimental data. The importance of including a continuous form of the clipped Gaussian PDF and the anisotropic turbulent characteristic is delineated in this test problem.

Turbulent Mixing in an SDR Combustor (Nonreacting Flow Case)

Simulation of turbulent mixing processes in a laboratory SDR combustor[8] is performed with no chemical reaction. In the experiments,[8] the two-dimensional SDR combustor comprised the main chamber, the fuel-injector nozzles, and the ram-air inlets, as shown in Fig. 4. Fuel-rich gases present in a practical SDR gas generator were simulated by cold air. Operating conditions were controlled so that the fuel nozzles were always choked, and the combustor was operated at a pressure of about 1 atm. The flow conditions at the fuel-injector nozzles were U_F = 313 m/s, V_F = 0, P_F = 1.7 atm, and T_F = 245 K. High-speed ram air was introduced into the main chamber at an inclined angle, with flow conditions of U_A = 122 m/s, V_A = −103 m/s, P_A = 1.24 atm, and T_A = 273 K. The measured velocity data at different cross sections is adopted for comparison with the results of present simulations.

Due to its symmetric geometry, only the upper-half plane of the combustor is selected as the computational domain. Computations with the inclusion of the clipped Gaussian PDF for thermodynamic-property fluctuations are performed in the Cartesian grid system. The transverse grid lines are clustered

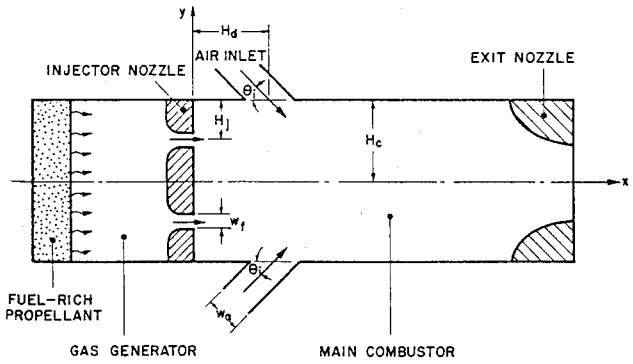

H_c	H_d	H_j	θ_i	w_a	w_f
63.5	58.1	31.75	45°	14.5	2.2

unit: mm

Fig. 4 Schematic of an SDR module combustor.

near the fuel-injector nozzle, the centerline, and the wall. All calculations addressed below are performed based on a 40 × 40 grid system, and the grid effect is justified by calculations based on the more dense grid systems presented later in this section.

Calculations with k-ε modeling show three recirculation zones which appear in Fig. 5a. Two stronger recirculations exist in the dome region, and one weaker one immediately downstream of the ram air slot. Due to the expansion processes through the fuel injector and the air slot, the two recirculations in the dome region are strong, each containing more than 30% of total mass flow rates. The third recirculation immediately downstream of the ram air slot is caused by reattachment of the ram air jet to the combustor wall. Figure 5b shows the low-pressure regions corresponding to the recirculation zones. The mixture fraction field is similar to the temperature field, as shown in Figs. 5c and 5d. This is not surprising, because the specific heat is almost linear to the temperature in this cold flow case, and both the governing equations and boundary conditions for the specific heat and mixture fraction are identical. Figure 5c shows that the most violent mixing occurs slightly upstream of the ram air inlet, due to the strong interaction between the fuel and the air jets. It is also apparent from Fig. 5e that large density variations are associated only with the corner recirculation zone, indicating that the fuel and air streams are mainly mixed in this region.

Enhancement of Predictions—ASM

Since the flowfield inside the SDR combustor involves mixing of high-speed streams and is characterized by multirecirculation zones, the turbulence structure is presumed to be highly inhomogeneous and anisotropic. Calculations with algebraic stress models are performed, and the predicted velocity profiles are compared at different cross sections with measurements[8] and previous results obtained through the k-ε model. For the ASM calculation, two sets of the ASM model constants are tested: $C_{r1} = 2.2$ and $C_{r2} = 0.7$, and $C_{r1} = 1.8$ and $C_{r2} = 0.6$. The former was proposed by Sultanian[31] with the calibration against the pipe flow data of Laufer,[32] and the latter was proposed by Gibson and Launder[33] to account for the anisotropic turbulence due to wall and streamline curvature effects. The corresponding ASM predictions hereafter are denoted as ASM-1 and ASM-2.

Profiles of the axial mean velocity predicted by the k-ε model and by the two ASMs are compared with LDV measurements[8] at eight typical cross sections in Fig. 6. In the dome region, where $X = 30$ and 45 mm, the ASM-2 predictions are better than those obtained by the ASM-1 and k-ε model. Downstream of the ram air jet, i.e., the region with

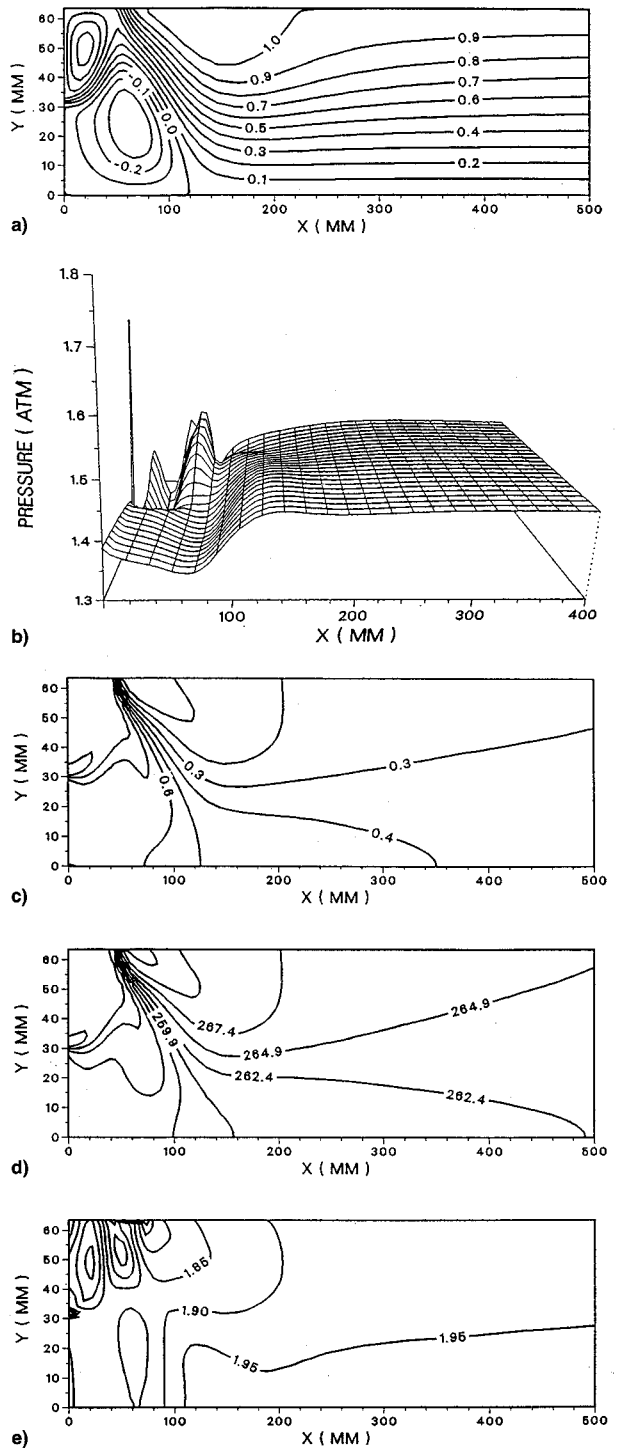

Fig. 5 Predictions in an SDR combustor, nonreacting flow case: a) streamline pattern, b) pressure field, c) mixture-fraction field, d) temperature field, and e) density field.

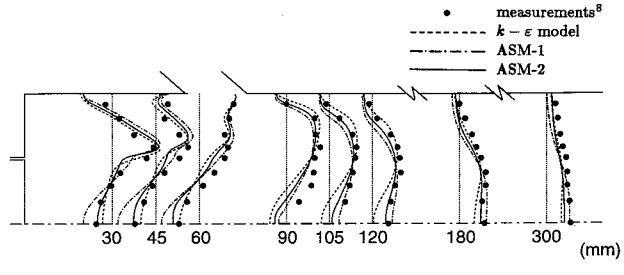

Fig. 6 Axial-velocity profiles measured[8] and calculated by different turbulence models, nonreacting flow case.

the upper-wall recirculation zone, the ASM-1 predicts as well as the ASM-2, but the k-ε model is less satisfactory. As for the region further downstream, i.e., the redeveloping region, all three models are equally satisfactory. As noted previously, the ASM-1 yields poor predictions in the dome region due to the existence of strong pressure variations that deviate greatly from the pipe flow characteristics. By the same token, better predictions by the ASM-1 after the dome region are caused by gradual exhibition of the pipe-flow characteristics in the flow. In general, the k-ε model cannot produce satisfactory results for any region except the redeveloping region. Also, it appears that ASM-2, i.e., the ASM with Gibson and Launder's model constants, seems to be a more adequate turbulence model for calculation of the SDR combustor flow.

Enhancement of Predictions—Compressible Turbulence Effects

In addition to the use of the clipped Gaussian PDF, the effects of compressible turbulence on modeling are considered here. Studies of compressible turbulence[34–36] are reviewed first. In contrast to the common use of the ratio of rms fluctuating density and mean density, the turbulent Mach number was considered to be an indicator by Erlebacher et al.,[34] Sarkar et al.,[35] and Sarkar[36] for the contribution of fluid dilatation to turbulence. Erlebacher et al.,[34] studying the low-speed flow (Mach number ≤ 0.3) by means of the asymptotic theory, showed that divergence of an initially incompressible velocity field grows rapidly on a nondimensional time scale of the order of the turbulent Mach number. Formulas were derived that accurately predict the level of compressibility after the initial transients have disappeared. Additionally, direct numerical simulation (DNS) for isotropic turbulence that verified the results from asymptotic theory was performed. Sarkar et al.[35] found that an equipartition exists between the turbulent kinetic and the potential components of the compressible energy for the low Mach number flow. DNS was also performed for isotropic turbulence, and results revealed that the above description holds for turbulent Mach numbers ranging from 0.01 to 0.5; i.e., it holds for both the low Mach number and the moderate Mach number flows. Based on the equipartition between the turbulent kinetic and the potential components of the compressible energy, a modification of the transport equation of turbulent kinetic energy (which includes the effects of compressible dissipation and pressure dilatation) was proposed by Sarkar et al.[35] One of the major concerns in predicting the SDR flow lies in the dome region, where the high-speed fuel gas interacts strongly with the side-inlet airstream and induces complicated flow phenomena and high-turbulent fluctuations. In this region, the high-speed fuel jet mixes violently with air; the flame is also anchored here. The turbulent Mach number is expected to be high in this region and in regions of violent combustion. The proposed modification by Sarkar et al.[35] is adopted in this study to account for the effect of compressible turbulence in the present SDR flows. An extra term is added to the transport equation of turbulent kinetic energy:

$$\nabla\cdot(\rho \boldsymbol{U} k) - \nabla\cdot(\Gamma_k \nabla k) = G_k - C_D \rho\varepsilon + (-\alpha M_t^2 \rho\varepsilon) \quad (15)$$

where

$$M_t = \sqrt{2k}/\bar{a} \quad (16)$$

Note that the symbol $\bar{a}$ denotes the local speed of sound, and 1 is the value of the model constant α.

Calculations with the modification in the k-ε model and the ASM-2 are performed, respectively. Predictions of mean axial velocities are shown in Fig. 7. Here, one notes obvious and significant improvement of the revised k-ε model over the standard one. Note also the proposed value 1 by Sarkar et al.[35] for the model constant α is based on the DNS for a decaying isotropic flow. As for anisotropic turbulence modeling, it appears that results of the revised ASM-2 are superior to those of the revised k-ε model in the dome region, but the improvement is not as significant for the entire flow field. From Figs. 6 and 7, it also appears that both the non-revised ASM-2 and the revised ASM-2 yield almost the same predictions. Based on the suggestion of Sarkar,[36] another optimal value 0.5 for α based on DNS of homogeneous shear flow, it appears that the constant α is subject to optimization. The applicability of the modification in the low turbulent Mach number regions for the present SDR flow can be validated by noting the results presented in Fig. 7. In the downstream low-turbulent Mach number regions in Fig. 7, the results with the inclusion of modification in the model still present satisfactory predictions. The turbulent Mach number distribution in the combustor flowfield also examined (not shown in the figure) found regions of substantial turbulent Mach number (i.e., higher than 0.3).

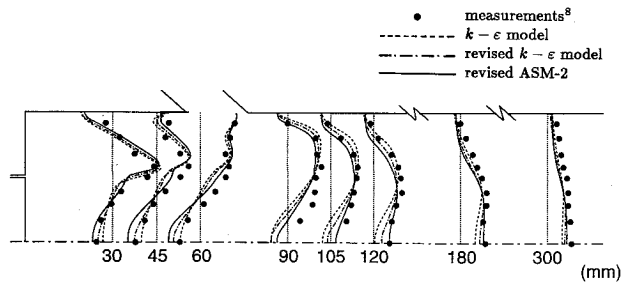

Fig. 7 Predicted axial-velocity profiles with revision of compressibility effect in turbulent models, nonreacting flow case.

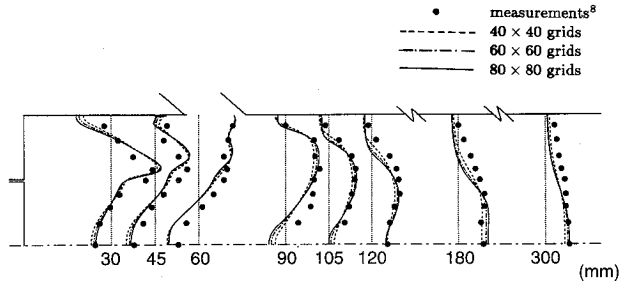

Fig. 8 Grid number effects on predicted axial-velocity profiles, nonreacting flow case.

So far, calculations are based on a 40 × 40 grid system. To assess the grid-number effects, the 60 × 60 and 80 × 80 grid systems are used to justify the previous results. Results of calculations with the ASM-2, including compressible turbulence modification, are shown in Fig. 8. In general, results with the 60 × 60 and 80 × 80 grid systems are almost identical in trend to those with the 40 × 40 system. No significant improvement can be found as the grid number is increased from 40 × 40. Thus, the 40 × 40 grid system is considered adequate for the present cases.

Turbulent Reacting Flow in an SDR Combustor

The same SDR combustor configuration is adopted for further consideration of the turbulent reacting flows. In the experiments,[8] propane gas was used instead of the solid propellant because its combustion behavior is more similar to that of the actual SDR propellant, which is easy to handle in simulation experiments. In the computer simulation, fuel-rich propane gas used in experiments is replaced by the mixture of propane and nitrogen, with the same mass fraction of propane, because the combustion model used here cannot allow the coexistence of fuel and oxidant. For the calculation of this reacting flow case, uniform flow conditions at the fuel injector are assumed to be $U_F = 569$ m/s, $V_F = 0$, $P_F = 7$ atm, $T_F = 1021$ K, $\tilde{f} = 1$, $g = 0$, $Y_{f,F} = 0.294$, $Y_{\text{in},F} = 0.706$, $\overline{v^1v^1} = (\frac{2}{3} + 0.3)k_F$, $\overline{v^2v^2} = (\frac{2}{3} - 0.18)k_F$, $\overline{v^3v^3} = (\frac{2}{3} - 0.12)k_F$,

and $\overline{v^1v^2} = 0.33k_F$. Uniform flow conditions at the ram air inlet are assumed to be $U_A = 92.73 \cos 45$ deg m/s, $V_A = -92.73 \cos 45$ deg m/s, $P_A = 5.84$ atm, $T_A = 535$ K, $\bar{f} = 0$, $g = 0$, $Y_{0,A} = 0.233$, $Y_{\text{in},A} = 0.767$, $\overline{v^1v^1} = (\frac{2}{3} + 0.3)k_A$, $\overline{v^2v^2} = (\frac{2}{3} - 0.18)k_A$, $\overline{v^3v^3} = (\frac{2}{3} - 0.12)k_A$, and $\overline{v^1v^2} = 0.33k_A$. The ASM, including the modification[35] for the compressible turbulence effects, is used with the model constants proposed by Gibson and Launder.[33] The clipped Gaussian PDF is also used to solve the temperature and the density distributions.

Calculations based on a 40 × 40 Cartesian grid system are performed first. Based on the predicted results, a 40 × 40 curvilinear streamline grid system is generated. Calculation is implemented again, based on this streamline grid system. The prediction based on streamline grids is given, and some comparison is made between the use of streamline grids and Cartesian grids for the flowfields.

Predictions of Mach number and pressure fields in an SDR combustor with chemical reaction involved are shown in Figs. 9a and 9b. A violent expansion is observed in the immediate downstream region of the sonic fuel injector. The expansion process proceeds and is accomplished before $X = 80$ mm. Rapid variations of flow properties also occur in the central recirculation zone. Pressure is almost uniform in the corner of the dome region and immediate downstream of the ram air slot. Behind the dome region, the Mach number field is generally less than 0.2 and is almost uniform throughout the combustion chamber.

For comparison, the predicted flow pattern based on the Cartesian grid system is given in Fig. 10a, and the streamline grid system and predicted flow pattern based on the streamline grid system is shown in Figs. 10b and 10c. As illustrated in Fig. 10b, transverse grid lines are generally aligned with flow directions. Due to the chemical reaction involved, part of the airstream is entrained toward the upstream fuel injector and mixed with the fuel stream (see Fig. 10a or 10c). The corner recirculation zone in the dome region is much weaker than that in the previous nonreacting flow case. Also, both the centerline recirculation zone and the upper-wall recirculation zone are much smaller than that in the cold flow case. As for the effects of grid adaption, observation of the evolution of ram air jets shown in Figs. 10a and 10c show that streamline grids give a steeper and deeper penetration prediction than do Cartesian grids. It is believed that a good alignment of grid lines with flow directions can help to reduce numerical diffusion errors. Less numerical diffusion error results in less smearing of the ram air jet and the recirculation strength. Figure 11a shows the predicted mean value of the mixture fraction using the Cartesian grid system, and both the predicted contours of mean and variance of the mixture fraction, based on the streamline grid system, are shown in Figs. 11b and 11c. It is noted that the contour $\bar{f} = 0.18$, corresponding to the stoichiometric value, represents the mean location of the flame sheet. In observing the locations of the contour $\bar{f} = 0.18$ in Figs. 11a and 11b, one notes that the flame sheet distribution is curved steeply in the dome region, behind which the flame sheet almost follows the developing trajectory of the ram air jet. The severe fluctuations of the mixture fraction are mainly caused by the expansion process of the ram air injection and the impingement of ram air and the fuel streams (see Fig. 11c). As for the effect of grid adaption, Fig. 11b shows that the streamline grid system gives a prediction of flame sheet distribution with a steeper skewness in the dome region than does the Cartesian grid system (see Fig. 10a). The streamline grid system presents that the developing flame sheet will extend to the outlet of the combustion chamber; however, Cartesian grid system predicted that it will attach to the upper wall. Thus, proper application of the curvilinear streamline grid system in the calculation to reduce numerical diffusion error is of vital importance to the prediction of turbulent reacting SDR flow properties. The mean isotherms of

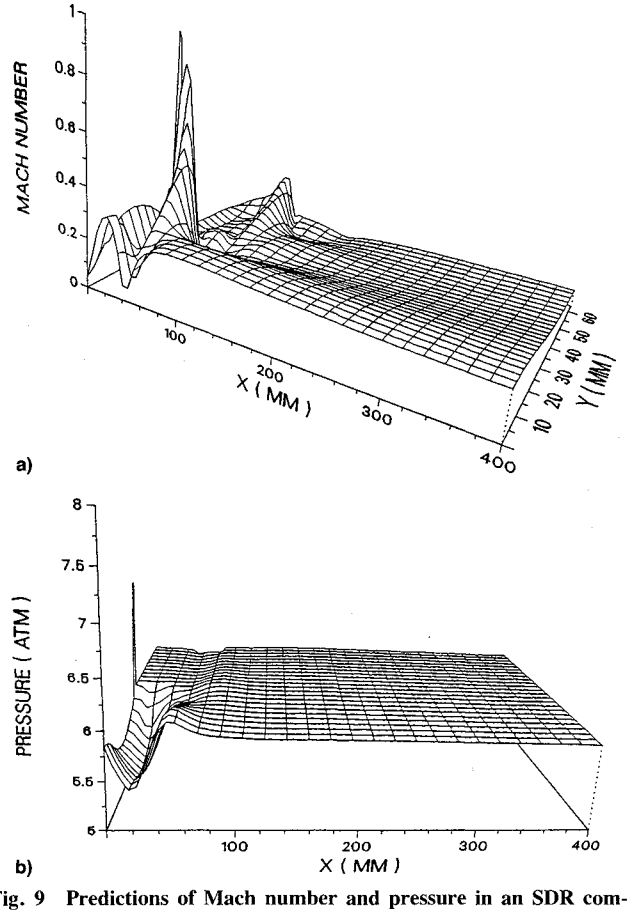

Fig. 9 Predictions of Mach number and pressure in an SDR combustor, reacting flow case: a) Mach number and b) pressure field.

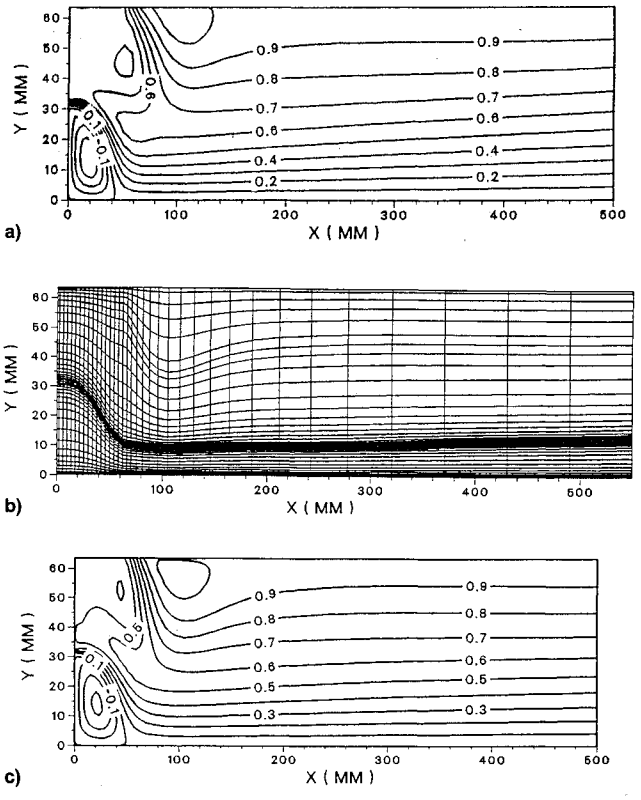

Fig. 10 Predictions of a streamline pattern in an SDR combustor and grid system used, reacting flow case: a) streamline pattern predicted by using the Cartesian grid system, b) streamline grid system generated by data of a), and c) streamline pattern predicted by using streamline grid system.

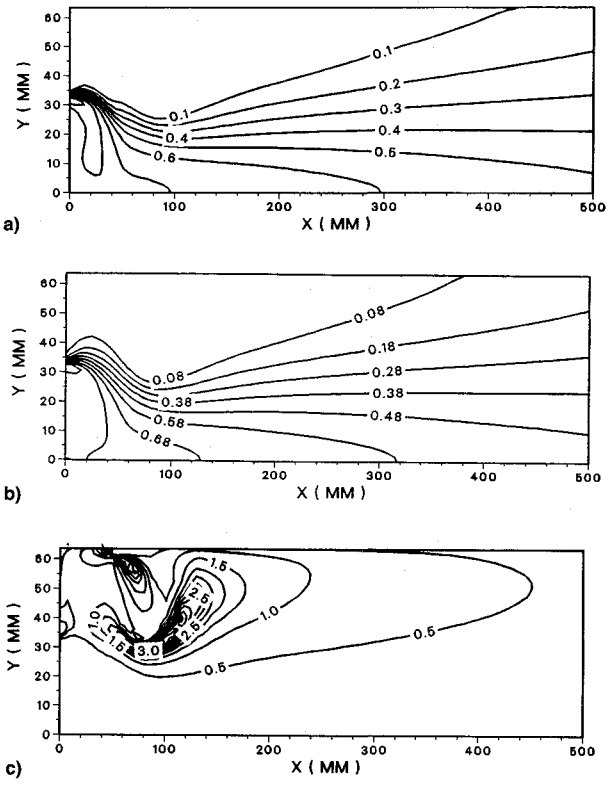

Fig. 11 Predictions of mixture fraction in an SDR combustor, reacting flow case: a) mean value predicted by use of Cartesian grid system, b) mean value, and c) intensity of fluctuation predicted by use of streamline grid system.

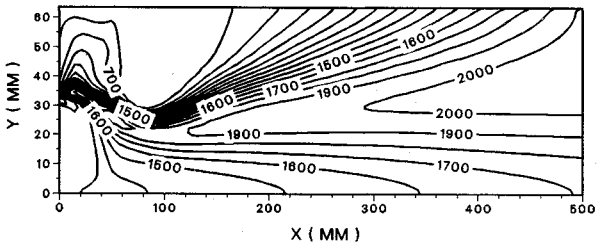

Fig. 12 Temperature distribution in an SDR combustor, reacting flow case.

this reacting flowfield are shown in Fig. 12. The maximum temperature gradient is found near the region across from the flame sheet, and the maximum temperature occurs near the skewed flame sheet in the dome region. The higher-temperature region is predicted to be located at the fuel-rich side of the flame sheet.

Summary and Conclusions

Computations of turbulent reacting flows are achieved in the general curvilinear coordinate system with the k-ε and algebraic stress turbulence models. Presumed forms of clipped Gaussian PDF are adopted to include the effect of fluid-property fluctuations. A streamline grid system is generated to perform the calculation of turbulent reacting flow in the SDR main combustor. A comparison of predictions using the Cartesian grid and those using streamline grid systems is made, and the importance and superiority of the streamline grid systems is delineated. The ASM with model constants proposed by Gibson and Launder, incorporated with compressible turbulence modification on the turbulent-kinetic-energy equation, is found to be more suitable for calculation of complicated SDR flows.

Acknowledgment

This research was partially supported by the National Science Council through Grant CS79-0210-D007-34. The financial support of this research is sincerely appreciated.

References

[1]Schadow, K. C., "Experimental Investigation of Boron Combustion in Air-Augmented Rockets," *AIAA Journal*, Vol. 7, No. 10, 1969, pp. 1870–1876.

[2]Schadow, K. C., "Boron Combustion in Ducted Rockets," AGARD-CP-307, Oct. 1981.

[3]Zetterström, K. A., Sjöblom, B., and Jarnmo, A., "Solid Ducted Rocket Engine Combustor Tests," *Proceedings of the Sixth International Symposium of Air Breathing Engines*, 1983, pp. 9–16 (ISABE Paper 83-7001).

[4]Zetterström, K. A., and Sjöblom, B., "An Experimental Study of Side Dump Ramjet Combustors," *Proceedings of the Seventh International Symposium of Air Breathing Engines*, 1985, pp. 169–176 (ISABE Paper 85-7024).

[5]Stull, F. D., Craig, R. R., Streby, G. D., and Vanka, S. P., "Investigation of Dual Inlet Side Dump Combustor Using Liquid Fuel Injection," AIAA Paper 83-0420, Jan. 1983.

[6]Nosseir, N., and Behar, S., "The Flowfield of Side-Dump Combustor," *Proceedings of the 22nd JANNAF Propulsion Meeting*, Vol. 1, CPIA 432, 1985, pp. 289–294.

[7]Liou, T. M., and Wu, S. M., "Flow Fields in a Dual-Inlet Side-Dump Combustor," *Journal of Propulsion and Power*, Vol. 4, No. 1, 1988, pp. 53–60.

[8]Chuang, C. L., "Experimental Study of Mixing and Combustion Processes in a Solid-Propellant Ducted Rocket Motor," Ph.D. Dissertation, Pennsylvania State Univ., University Park, PA, 1989.

[9]Chen, L., and Tao, C. C., "Study of Side-Inlet Dump Combustor of Solid Ducted Rocket with Reacting Flow," AIAA Paper 84-1378, June 1984.

[10]Cherng, D. L., Yang, V., and Kuo, K. K., "Numerical Study of Turbulent Flows in Solid-Propellant Ducted Rocket Combustors," *Journal of Propulsion and Power*, Vol. 5, No. 6, 1989, pp. 678–685.

[11]Liou, T. M., and Hwang, Y. H., "Calculation of Flow Fields in Side-Inlet Ramjet Combustor with an Algebraic Reynolds Stress Model," *Journal of Propulsion and Power*, Vol. 5, No. 6, 1989, pp. 686–693.

[12]Khalil, E. E., Spalding, D. B., and Whitelaw, J. H., "The Calculation of Local Flow Properties in Two Dimensional Furnaces," *International Journal of Heat and Mass Transfer*, Vol. 18, No. 6, 1975, pp. 775–791.

[13]Bilger, R. W., and Kent, J. H., "Concentration Fluctuations in Turbulent Jet Diffusion Flames," *Combustion Science and Technology*, Vol. 9, No. 1, 1974, pp. 25–29.

[14]Spalding, D. B., "Concentration Fluctuations in a Round Turbulent Free Jet," *Chemical Engineering Science*, Vol. 26, No. 1, 1971, pp. 95–107.

[15]Naguib, A. S., "The Prediction of Axisymmetrical Free Jet, Turbulent Reacting Flows,"Ph.D. Dissertation, Univ. of London, 1975.

[16]Richardson, J. N., Howard, H. C., Jr., and Smith, R. W., Jr., "The Relation Between Sampling-Tube Measurements and Concentration Fluctuations in a Turbulent Gas Jet," *Proceedings of the 4th Symposium (International) on Combustion*, 1953, pp. 814–817.

[17]Odidi, A. O. O., "The Influence of Turbulence on the Time Mean Rate of Reaction," Ph.D. Dissertation, Univ. of London, 1974.

[18]Bilger, R. W., and Beck, R. E., "Further Experiments in Turbulent Jet Diffusion Flames," *15th Symposium (International) on Combustion*, 1975, pp. 541–552.

[19]Elghobashi, S. E., "Characteristics of Gaseous Turbulent Diffusion Flames in Cylindrical Chambers, A Theoretical and Experimental Investigation," Ph.D. Dissertation, Univ. of London, 1975.

[20]Khalil, E. E., *Modelling of Furnace and Combustors*, Abacus Press, Kent, England, UK, 1982, pp. 57–72.

[21]Rodi, W., "A New Algebraic Relation for Calculating the Reynolds Stresses," *ZAMM*, Vol. 56, 1976, pp. T219–T221.

[22]Chao, Y. C., and Liu, S. S., "Streamline Adaptive Grid Method for Complex Flow Computation," *Numerical Heat Transfer*, Vol. 20, Pt. B, 1991, pp. 101–124.

[23]Launder, B. E., and Spalding, D. B., "The Numerical Computation of Turbulent Flows," *Computer Methods in Applied Mechanics and Engineering*, Vol. 3, No. 2, 1974, pp. 269–289.

[24]Shyy, W., Tong, S. S., and Correa, S. M., "Numerical Recir-

culating Flow Calculation Using a Body-Fitted Coordinate System," *Numerical Heat Transfer*, Vol. 8, No. 1, 1985, pp. 99–113.

[25]Van Doormaal, J. P., and Raithby, G. D., "Enhancements of the SIMPLEC Method for Predicting Incompressible Fluid Flow," *Numerical Heat Transfer*, Vol. 7, 1984, pp. 147–163.

[26]Demirdzic, I., Gosman, A. D., Issa, R. I., and Peric, M., "A Calculation Procedure for Turbulent Flow in Complex Geometries," *Computers and Fluids*, Vol. 15, No. 3, 1987, pp. 251–273.

[27]Eiseman, P. R., "Adaptive Grid Generation," *Computer Methods in Applied Mechanics and Engineering*, Vol. 64, No. 1, Pt. B, 1987, pp. 321–376.

[28]Lockwood, F. C., El-Mahallawy, F. M., and Spalding, D. B., "An Experimental and Theoretical Investigation of Turbulent Mixing in a Cylindrical Furnace," *Combustion and Flame*, Vol. 23, No. 3, 1974, pp. 283–293.

[29]Hanjalic, K., and Launder, B. E., "A Reynolds Stress Model of Turbulence and its Application to Thin Shear Flows," *Journal of Fluid Mechanics*, Vol. 52, Pt. 4, 1972, pp. 609–638.

[30]Launder, B. E., Reece, G. J., and Rodi, W., "Progress in the Development of a Reynolds-Stress Turbulence Closure," *Journal of Fluid Mechanics*, Vol. 68, Pt. 3, 1975, pp. 537–566.

[31]Sultanian, B. K., "Numerical Modeling of Turbulent Swirling Flow Downstream of an Abrupt Pipe Expansion," Ph.D. Dissertation, Arizona State Univ., Tempe, AZ, 1984.

[32]Laufer, J., "The Structure of Turbulence in Fully Developed Pipe Flow," NACA TN 2954, June 1953.

[33]Gibson, M. M., and Launder, B. E., "Ground Effects on Pressure Fluctuations in the Atmospheric Boundary Layer," *Journal of Fluid Mechanics*, Vol. 86, Pt. 3, 1978, pp. 491–511.

[34]Erlebacher, G., Hussaini, M. Y., Kreiss, H. O., and Sarkar, S., "The Analysis and Simulation of Compressible Turbulence," *Theoretical and Computational Fluid Dynamics*, Vol. 2, No. 2, 1990, pp. 73–95.

[35]Sarkar, S., Erlebacher, G., Hussaini, M. Y., and Kreiss, H. O., "The Analysis and Modeling of Dilatational Terms in Compressible Turbulence," *Journal of Fluid Mechanics*, Vol. 227, June 1991, pp. 473–493.

[36]Sarkar, S., "Modeling of the Pressure-Dilatation Correlations," Inst. for Computer Applications in Science and Engineering, ICASE Rept. No. 91-42, May 1991.